Novel Nanofibrillated Cellulose/Chitin Whisker Hybrid Nanocomposites and their Use for Mechanical Performance Enhancements

Yucheng Feng,† Jinpeng Li,† Bin Wang,* Xiaojun Tian, Kefu Chen, Jinsong Zeng, Jun Xu, and Wenhua Gao

The aim of this work was to demonstrate the production potential of a combination of the two materials cellulose nanofibrils (CNF) and chitin nanowhisker (CNW) using wheat straw and chitin. CNF and CNW were prepared from TEMPO-oxidation and acid hydrolysis prior to high-pressure homogenization. The zeta potential results indicated the differences in the suspended mechanism for the CNF and CNW dispersions. Fourier transform infrared spectroscopy (FTIR) and X-ray diffraction (XRD) revealed that the chemical composition and crystal unit changes during the chemical separation process. Hybrid CNF/CNW films were prepared *via* casting and evaporation. The films had better mechanical properties, which were ascribed to multivalent physical interactions between CNF and CNW. However, increasing the CNW content up to 50% negatively affected the mechanical properties of the hybrid films. In addition, all films showed high transparency and excellent flexibility. These results indicated that the interaction between CNF and CNW effectively enhanced the mechanical performance of films.

Keywords: Cellulose nanofibrils; Chitin nanowhisker; Nanocomposites; Mechanical properties

*Contact information: Plant micro/nano fiber Research Center, State Key Laboratory of Pulp and Paper Engineering, School of Light Industry and Engineering, South China University of Technology, Guangzhou 510640, China; *Corresponding author: febwang@scut.edu.cn. † Contributed equally to this work.*

INTRODUCTION

Agricultural and marine wastes are two of the least utilized classes of renewable resources in China, which is a big agricultural country (Chandra *et al*. 2012). The isolation of cellulose and chitin from renewable resources such as crop and shellfish residues are beneficial to industries and the environment due to their large quantities of raw materials and renewability (Shen *et al.* 2016). In recent decades, growing concerns for preserving the environment have resulted in an increase in the use of environmentally friendly materials to produce industrial products. Now a promising area is to more effectively use chitin, which is the next most available polysaccharide after cellulose and hemicellulose. In addition, chitin and cellulose are all renewable, biodegradable, and non-toxic.

Cellulose nanofibrils (CNF) are nanomaterials with widths on the nanometer scale and lengths often in the range 1 μm to 5 μm (Khalil *et al*. 2012). These nanomaterials have the advantageous properties of cellulose, including renewability, degradability, and worldwide availability. Therefore, nanomaterials show great potential for applications in many fields. Mechanical, enzymatic/mechanical, and chemical/mechanical methods have been applied as a means of isolating CNF from different resources (Huang *et al.* 2013; Fang *et al.* 2014). CNF has been used as a component in various fields including electronic

devices, tissue engineering, and energy storage (Zheng *et al*. 2013; Li *et al.* 2014). Although these materials possess excellent mechanical properties, the tightly packed random network structure shows typically brittle failure as cracks (Malho *et al*. 2014). Hence, some cross-linked polymers such as phenolic resins, epoxy, and melamine formaldehyde were mixed with CNF in the following work (Ansari *et al*. 2014; Nair *et al.* 2017; Diop *et al.* 2017). The consequent problems could occur due to rigid and brittle covalent bonds, which lead to losses in toughness (Ansari *et al*. 2014).

Chitin is a linear polysaccharide constituted of β-(1, 4)-linked N-acetylglucosamine (GlcNAc) units. Chitin nanowhiskers (CNW) have a highly uniform structure with lateral dimensions from 2.5 nm to 25 nm. The positive charge on the surface of chitin can react with negatively charged cellulose by static adsorption. Owing to the good film-forming performance, nano-scale CNW has a strong interaction with cellulose (Kumar *et al.* 2017).

Physical adsorption is a feasible way to form composite materials and retain their mechanical properties (Qiu *et al*. 2016). The CNF-based materials were prepared using polysaccharide carbohydrates and proteins, such as chitosan, chitin, and silk, which consist of various kinds of chemical bonds that can bond with the cellulose surface by physical or chemical interactions (Singh *et al.* 2013; Naseri *et al*. 2014). Due to physical adsorption and complementary properties of both cellulose and chitosan (*e.g*., hydrogen bonding between amide and hydroxyl groups, and electrostatic attraction between the positively charged and the negatively charged groups), some hybrid composites have been prepared and used in different areas, such as anti-microbial and oxygen barrier materials (Singh *et al.* 2013; Kingkaew *et al*. 2014; Mututuvari and Tran 2014). Toivonen provided a new method to prepare a CNF/chitosan nanopaper, which showed excellent mechanical properties under a wet moist environment (Toivonen *et al*. 2015). However, the agglomeration of cellulose/chitosan composites has been found to occur, especially at a higher level of chitosan loading; this led to a decrease in mechanical properties (Abdul *et al.* 2016).

In this study, chitin nanowhiskers were used to reinforce the CNF nanofilms. First, CNF was mixed with CNW to form homogeneous and aqueous mixtures. The chemical bonds within the intramolecular and intermolecular of CNF and CNW were investigated by Fourier transform infra-red (FTIR) spectra. Additionally, the mixed film was easily cast and highly transparent. Its mechanical and thermodynamic properties were evaluated.

EXPERIMENTAL

Materials

Wheat straw was provided by Shandong Tranlin Group Co., Ltd. (Shandong, China). Cellulosic fiber (α-cellulose ≥ 95%) was obtain from wheat straw (Supplementary information 1, S1). α–Chitin was purchased from Yuan Ye BIO Ltd. (Shanghai, China). Analytical grade 2, 2, 6, 6-tetramethy-1piperidinyloxy (TEMPO) and sodium hypochlorite were used as received. Water at 18.2 MΩ was purified with a Millipore Milli Q system (Millipore Direct Q5, Merck, USA). All other chemicals were analytical reagent grade obtained from Sinopharm Chemical Reagent Co. (Shanghai, China) and used without further purification.

Preparation and characterization of CNF and CNW

Cellulosic fiber was oxidized under the TEMPO/NaClO/NaBr system at pH 10.2

to minimize hydrolysis of the polymeric structure. More detailed information is described in S2 (Supplementary information 2 in the Appendix). The carboxylate content of cellulose was investigated by conductometric titration (Supplementary information 3, S3) and the conductometric titration curve is shown in Fig. S1(a). Viscosity of nanofibers and the degree of polymerization (DP) was determined by S4 (Supplementary information 4).

Chitin nanowhiskers were prepared according to Li *et al*. (2015). Chitin was hydrolyzed under acidic conditions and then partially deacetylated in a NaOH solution (Supplementary information 5, S5). The C_2 amino content of CNW was determined by conductometric titration (Supplementary information 6, S6), and the conductometric titration curve are depicted in Fig. S1(b). Molecular weight and degree of deacetylation of CNW were determined by S7 (Supplementary information 7, S7).

Preparation of mixtures of CNF /CNW and film casting

The films of CNF and CNW were mixed and dispersed in different mass ratios and formed by a casting method (Supplementary information 8, S8). The films were marked as CNF-1 (pure CNF-1 film), CNF-2 (pure CNF-2 film), CNF-5 (pure CNF-5 film), CNW (pure CNW film), MIX-1 (CNF-2/CNW=70:30), MIX-2 (CNF–2/CNW=50:50) and MIX-3 (CNF-2/CNW=30:70).

Methods

Morphological analysis

Morphological features of CNF and CNW were determined by transmission electron microscopy (TEM). A homogeneous solution was obtained by sonication. Dilute CNF and CNW suspensions were dropped onto glow-discharged carbon-coated TEM grids and negatively stained with 2 wt.% uranyl acetate for 5 min. The samples were observed on TEM (Jeol, JEM-2100F, Tokyo, Japan).

To complement the TEM images, the hybrid film was observed by atomic force microscopy (AFM) with a multimode scanning probe microscope (MultiMode-8, Bruker Corporation, Billerica, MA) that was operated in tapping mode.

Zeta potential

The zeta potential of CNF and CNW solutions were measured using a Zeta sizer Nano ZS (Malvern Instruments, Malvern, UK). Cellulosic fiber and chitin whisker dispersions (0.30 wt.%) were previously dispersed with homogenizer for 5 min at 12000 rpm/min.

Fourier transform infrared spectroscopy (FTIR) measurement

The FTIR spectra for CNF, CNW, and film-samples were recorded with a Nexus 470 spectrophotometer (Thermo Nicolet, Madison, WI, USA). The samples were mixed and ground with KBr for IR measurements within the frequency range of 4000 cm^{-1} to 400 cm^{-1}.

X-ray diffraction

CNF, CNW, and CNF/CNW films were X-rayed using a D8 Advance diffractometer (Bruker, Daltonik GMBH, Bremen, Germany) with CuKα filtered radiation (λ = 0.154 nm) and was operated at 40 kV with a current density of 40 mA. The scanning range (2θ) was from 5° to 45° at a scan rate of 2°/s and a step width of 0.02°.

The crystal width was determined by the Scherrer equation (Eq. 1),

$$D = \frac{K\lambda}{\beta cos\theta} \quad (1)$$

where K is a constant equal to 0.9, λ is the wavelength of the radiation, θ is the diffraction angle, and β is the full width at half-maximum intensity. According to the previous work (Wada *et al*. 2001), the Z value was determined to discriminate the I_α and I_β dominant structures, given by Eq. 2,

$$Z = 1693d_1 - 902d_2 - 549 \quad (2)$$

where d_1 and d_2 are the d-spacings marked in XRD profile.

Mechanical test

The films were cut into 10 mm × 80 mm strips. The mechanical tests were performed with an Instron 5565 testing machine (Inston, Canton, MA, USA) using 0.1 kN power sensor at a crosshead rate of 10 mm/min in a constant temperature and humidity facilities. Film thicknesses were measured with a thickness tester (L&W, SE51, Stockholm, Sweden), and the thickness of each film was determined as an average of ten measurements.

Thermogravimetric analysis (TGA)

The TGA of films was performed with a NETZSCH TG 209 Jupiter Thermal Analysis System (TA Instruments, New Castle, DE, USA) thermogravimetric analyzer under an air atmosphere (50 mL/min). The samples were heated from 25 °C to 650 °C at a heating rate of 10 °C/min.

Porosity

The film porosity was determined by measuring the wet film weight in deionized water overnight at room temperature and the dry membrane was weighted after drying in a vacuum oven at 50 °C for 24 h (Supplementary information 9, S9).

RESULTS AND DISCUSSION

Preparation and Characterization of CNFs and CNW

The degree of polymerization (DP) of the CNF presented a descending trend according to the viscosity data shown in Table 1. The reduction of DP in TEMPO-oxidized cellulose was consistent with Zhang *et al*. (2012). When the amount of NaClO was raised to 9 mmol/g, the DP decreased by approximately 25%.

The carboxylate content of the TEMPO-oxidized fiber was investigated with the addition of different amounts of NaClO. The carboxylate content of CNF was remarkably increased from 0.59 mmol/g to 0.95 mmol/g at 1.5 and 9.0 mmol/g of NaClO, respectively. The change in zeta potential from -32.9 mV to -48.1 mV indicated that more carboxylate was formed on the fiber surface. Therefore, in the oxidation process, hypochlorite promotes the conversion from alcoholic hydroxyls to carboxyls in cellulose units (Zhang *et al*. 2016).

All the prepared CNF and CNW were easily suspended in aqueous solution to achieve a well-dispersed suspension. The zeta potential of CNF and CNW suspensions were then detected, and the results were different, as shown in Table 1. Therefore, the nano-dispersion mechanisms of TEMPO-oxidized CNF and acid hydrolyzed CNW were different. CNF dispersed in water by anionic C6-carboxylated groups, which were formed

by TEMPO oxidation on the glucose unit surface in CNF (Zhang *et al*. 2012). CNW dispersed in water by cationic C2-ammonuiun salt group on the N-acetylglucosamine units surface in CNW. The dispersed behaviors of the suspensions, when considered separately, were caused by charge repulsions between the positive electrical charges on CNW and the negative electrical charges on CNF.

Table 1. Physical and Crystal Structures for CNF and CNW with different Chemical Treatments

Samples	DP	Amino	Carbonyl	Zeta Potential	Morphology size		Crystal Unit		CrI
		Content (mmol/g)		(mV)	Length （nm）	Diameter （nm）	Length (nm)	Width (nm)	(%)
CNF - 1[a]	640	-	0.59	-32.9	416.3	26.4	9.1	4.3	53.2
CNF - 2[b]	560	-	0.60	-33.5	383.7	22.1	8.9	3.7	55.4
CNF - 5[c]	270	-	0.95	-48.1	274.9	14.5	7.5	3.2	61.9
Chitin	-	-	-	+17.3	-	-	8.4	5.7	44
CNW	54	0.94	-	+64.2	209.5	11.8	7.7	4.4	52

Note: Amount of hypochlorite added: *a*: 1.5 mmol/g; *b*: 3.0 mmol/g; *c*: 9.0 mmol/g

The viscosity average molecular weights (M_v) and degree of deacetylation (DD) of raw chitin were 8.41×10^5 and 16.1%. After the acid hydrolysis and N-deacetylation reaction, M_v of CNW was reduced to 1.15×10^4 and DD was raised to 54.16%. This indicated that the amorphous regions of chitin were destroyed in the acid hydrolysis process, and the molecular chains of chitin were broken into smaller chains. The DD values in the present work were less than the referenced values (Kaya *et al*. 2016). In addition, the partial deacetylation caused more intensive protonation and amino groups exposed on the surface of CNW (Li *et al*. 2016). Then higher values of positive zeta potential were shown in aqueous solution after N-deacetylation treatment, which is more conducive to get a stable dispersion system (Li *et al.* 2016).

Chemical Structural Analysis CNF and CNW

FTIR was employed to investigate the functional group, which further explained the correlation of chemical structure and dispersion characteristics of CNF and CNW suspensions, as shown in Fig. 1.

The absorption peak of CNW in the region around 3250 cm^{-1} was an indication of the stretching of -OH groups. The vibration absorption peaks ranging from 2900 cm^{-1} to 2800 cm^{-1} were anti-symmetric and symmetric -CH stretching vibrations (Li *et al*. 2015). The vibration absorption peak at 3460 cm^{-1} was attributed to the N-H stretching vibration, which resulted in a positive zeta potential of CNW in suspension liquid.

The FTIR spectra of CNF with different oxidation degrees are depicted in Fig. 1a. The spectra exhibited similar characteristic absorption peaks. The absorption peak in the range of 3650 cm^{-1} to 3000 cm^{-1} was assigned to the stretching of O-H, and the peak at 1600 cm^{-1} was attributed to the C=O stretching vibration of COO^-. The presence of the COO^- group indicated a negative surface charge on CNF surface in suspension liquid.

Moreover, a comparison of the intensity of the stretching vibration band at 1600 cm^{-1} was executed by the normalization of the FTIR spectrum (Fig. 1b). Due to the higher oxidation degree, the peak at 1600 cm^{-1} attributed to carboxylate group in CNF-5, was stronger than CNF-2 and CNF-1.

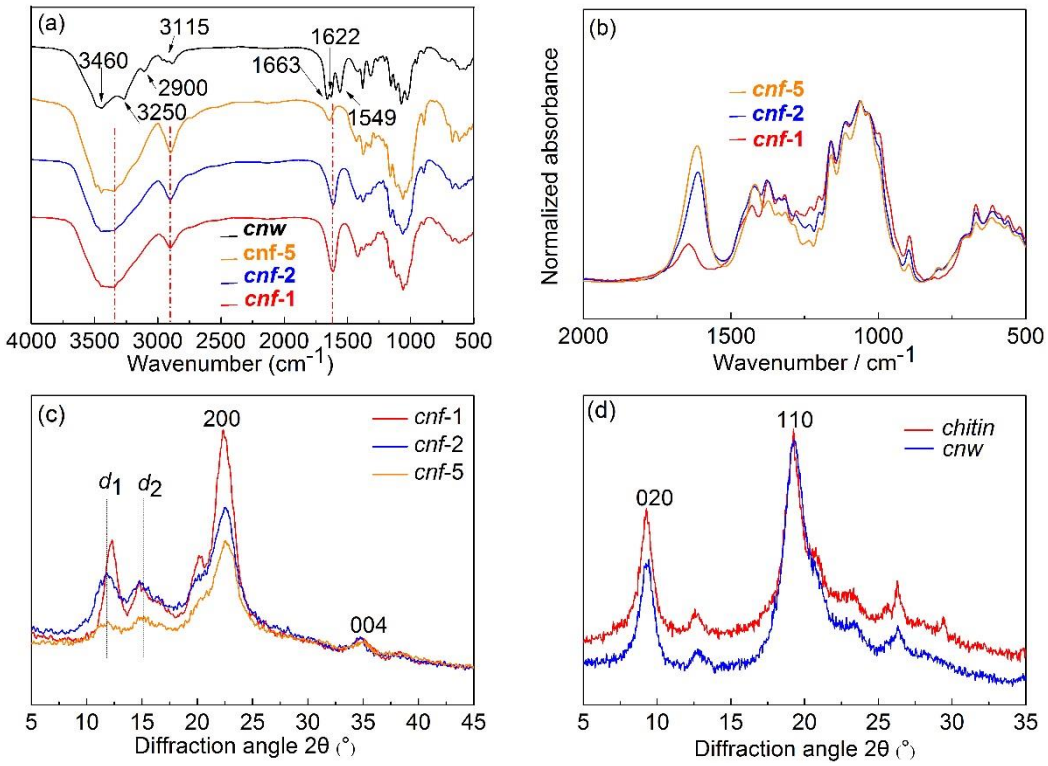

Fig. 1. (a) FTIR spectra of CNW and CNF (CNF-1, CNF-2, and CNF-5), (b) the spectra were normalized so that the peak heights of the bands were equal, (c) XRD profile of CNF, and (d) Chitin and CNW

XRD Analysis

The X-ray diffraction profiles of CNF and CNW were analyzed, and results are shown in Fig. 1 (c) and (d). The diffractions of CNF at 22.6º is related with (200) planes, which reveals a typical cellulose I crystalline form (Chen *et al.* 2011). The crystal width, Z value (to discriminate the I_α and I_β dominant structures) and degree of crystallinity (CrI) were determined according to S10 (Supplementary information 10).

A positive *Z* value manifested I_α structure and a negative *Z* value represented I_β structure. The Z value of -5.59 indicated that the prepared CNF belongs to I_β crystal structure. The crystal length and width of CNF-1 were 9.1 and 4.3 nm, determined from the (004) and (200) diffraction peaks, respectively, and the results are listed in Table 1. The aspect ratio of the cellulosic crystals was 2.1, which was lower than that of the wood cell wall (Marko *et al*. 2008).

Similarly, the crystal sizes of chitin were 8.4 and 5.7 nm, which was determined from the diffraction peaks at 9.6° and 19.6°, as shown in Fig. 1(d). The crystal sizes of CNW slightly decreased to 7.7 and 4.4 nm after acid hydrolysis. However, the CrI value of CNW increased after acid hydrolysis, which was from 0.44 to 0.52. A possible explanation is that hydrolysis mostly occurred on the amorphous region of α-chitin.

Morphological Analysis

Figure 2 shows TEM images of CNFs and CNW. It was revealed that nanofibers could easily form lateral aggregates due to their large specific surface area. Carboxylate groups on the surface of CNFs promoted the conversion of fibers into individual fibers

with uniform lateral size ranging from 10 nm to 15 nm. The diameter of CNF-5 sample was smaller than CNF-2 and CNF-1. The results indicated that TEMPO oxidation efficiently promoted cellulose nanofibrillation to individual nanofibrils (Liimatainen *et al*. 2012). Fig. 2(c) shows that more severely oxidized fibrils have smaller diameter and smaller size of CNF, which tends to form more transparent suspension, as shown in Fig. 2(e).

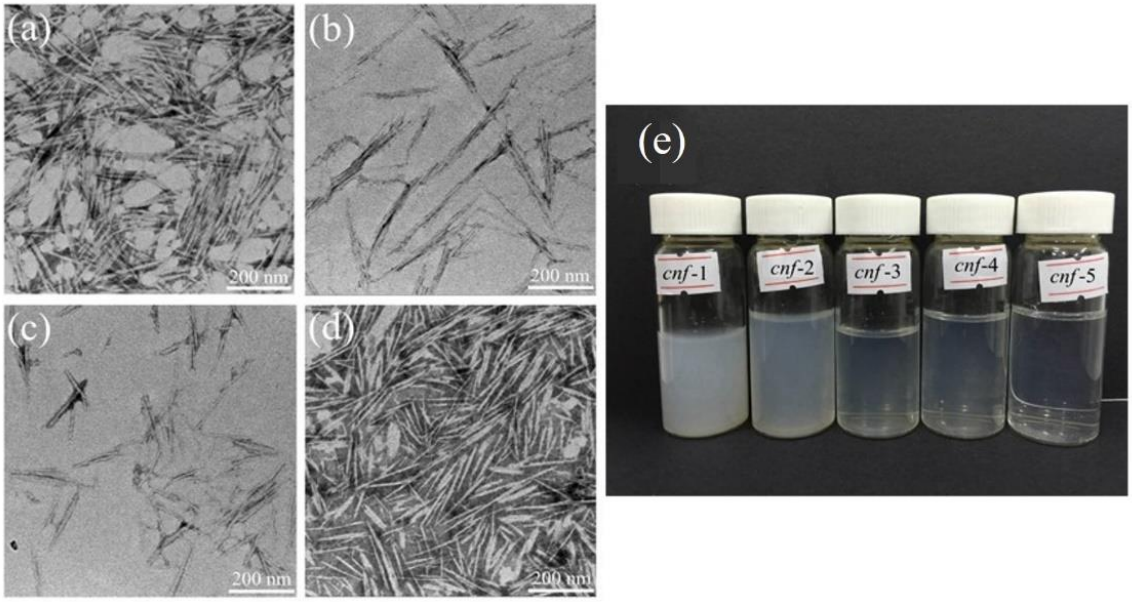

Fig. 2. TEM images of (a) CNF-1, (b) CNF-2, (c) CNF-5, (d) CNW, and (e) the suspension of CNF

Preparation and Characterization of Films

The goal was to prepare a hybrid nanofilms with the positively charged CNW and negatively charged CNF to improve the performances of the nanocomposites. Figure 3a shows the photographs of CNF-2, CNW, and MIX-2 films. There were obvious differences in transmittance of the films with different composition ratios, as shown in Fig. 3b. The films of CNF (CNF-5, CNF-2, and CNF-1) showed high transparencies in the range of 400 nm to 800 nm, which were between 60% and 80%.

Table 2. Physical and Mechanical Properties of the Films from CNF and CNW with Different Proportions

Samples	Thickness (μm)	Density (g/cm^3)	Tensile strength (MPa)		E-modulus		Elongation (%)	
			Dry[a]	Wet[b]	Dry[a] (GPa)	Wet[b] (MPa)	Dry[a]	Wet[b]
CNF-1	55.3	0.904	52.6 ± 3.4	2.5 ± 0.2	5.6 ± 0.2	28.3 ± 1.5	1.5 ± 0.1	3.8 ± 0.2
CNF-2	52.5	0.952	63.7 ± 2.8	6.4 ± 0.3	6.9 ± 0.2	34.7 ± 2.2	1.7 ± 0.1	4.1 ± 0.3
CNF-5	48.8	1.025	74.8 ± 3.2	10.6 ± 0.4	8.0 ± 0.3	36.2 ± 2.9	2.4 ± 0.2	4.5 ± 0.3
CNW	39.2	1.274	46.1 ± 1.4	8.6 ± 0.2	4.9 ± 0.2	38.4 ± 2.4	1.3 ± 0.1	2.1 ± 0.1
MIX-1	47.1	1.048	69.2 ± 2.9	8.5 ± 0.2	7.3 ± 0.3	37.1 ± 4.8	2.8 ± 0.2	4.3 ± 0.4
MIX-2	45.4	1.135	83.4 ± 3.5	9.2 ± 0.3	8.6 ± 0.4	43.5 ± 2.6	1.8 ± 0.1	2.4 ± 0.2
MIX-3	43.7	1.164	41.6 ± 1.7	3.0 ± 0.1	5.8 ± 0.2	26.2 ± 1.9	1.6 ± 0.1	1.6 ± 0.1

Note: Test Conditions: a: films were kept at 23 °C and relative humidity of 50% ± 1% for 24 h; b: films were kept at 23 °C and relative humidity of 98% ± 1% for 24 h.

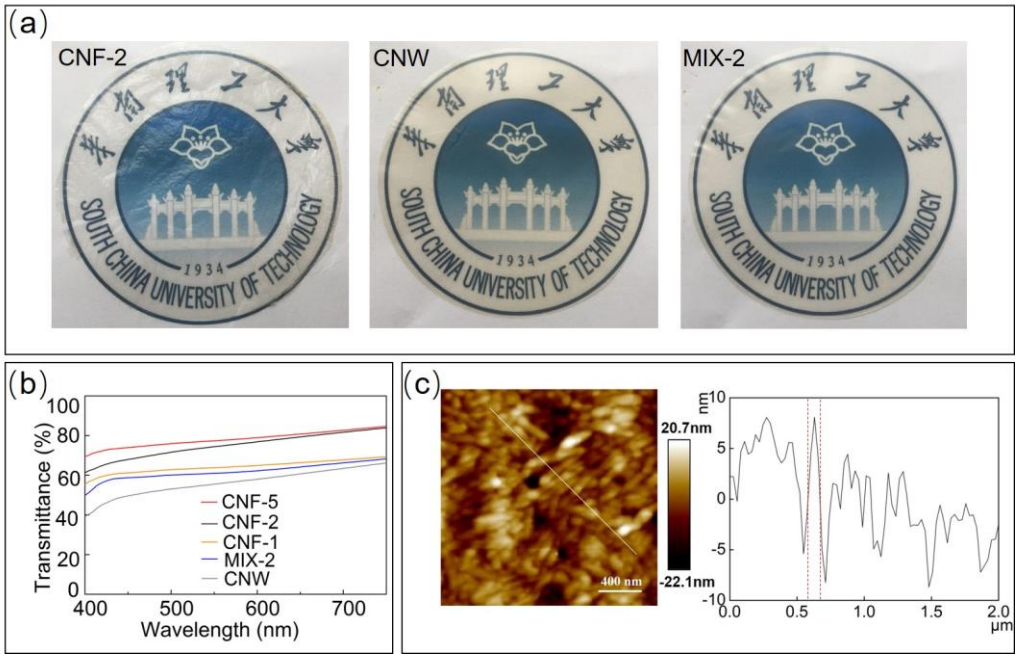

Fig. 3. (a) Photographs of films of CNF-2, CNW, and MIX-2, (b) UV-vis transmittance of nanofilms, (c) AFM image of composite film of MIX-2 scanned with size of 1 μm × 1 μm and the its height profile of lines.

The CNW film showed approximately 50% at 500 nm. The transparency of the composite film of MIX-2 was increased by an addition of CNF-2. Previous work has confirmed that the uniform sizes are beneficial for light transmission (Yano *et al.* 2005). Thus, introducing CNW into the composite film increased the particle size and negatively affected the light transmission.

The thickness, density, and mechanical properties of the hybrid films are listed in Table 2. All densities of the films were lower than CNF (1.6 g/ cm^3), and CNW (1.5 g/ cm^3) (Dufresne 2001; Saito *et al.* 2009). These results demonstrated that fine-scaled porous structures were present in the composite films. An apparent shrinkage in the sizes of hybrid films could be observed with the increasing of CNW. This was due to more hydrogen bonds having formed between CNF and CNW. The AFM images of MIX-2 film also offers an approximate overview of the CNFs and CNWs morphology in Fig. 3c. According to the AFM height image, the brighter colors indicate higher samples and darker colors represent lower (Zerson *et al*. 2016). MIX-2 showed a uniform distribution and the pore size in the films were clearly visible. The cross-sectional analysis of the representative interlaced nanofiber had a diameter of 89 nm, which is higher than CNF and CNW reflected by TEM images.

Effect of CNW on Porosity of Composite Film

Figure 4a shows the effect of mixing proportion on the porosity of CNF and CNW in the prepared films. The porosity of the films decreased with the increasing of TEMPO-oxidation. It is attributed to there being more carboxylate groups on the surface of CNF-5 (compared with CNF-1 and CNF-2), and these could form large number of hydrogen bond links, which decreased the pore size of pure CNF films. It was also revealed that the doped CNW increased the porosity of nanocomposite films.

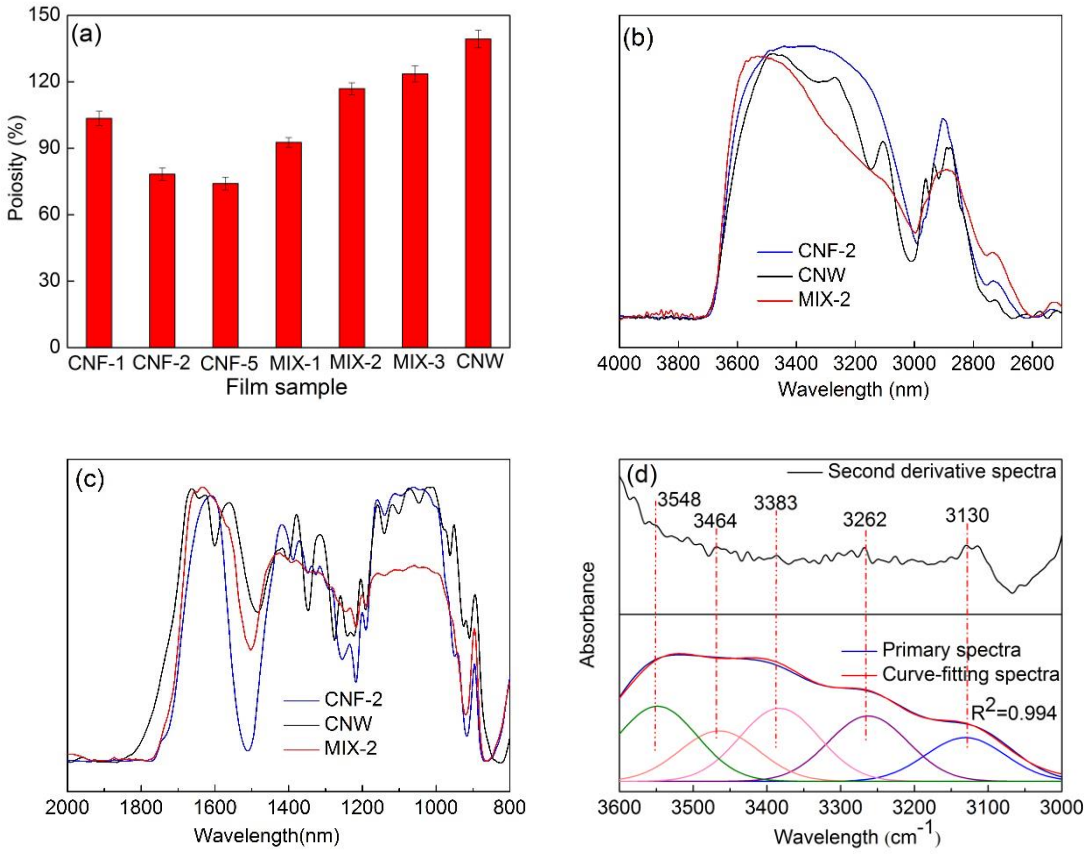

Fig. 4. (a) Porosity of hybrid films with different ratios of CNF and CNW, (b) (c) FTIR spectra of CNF-2, CNW and MIX–2, and (d) second derivative, primary and curve-fitting spectra of MIX–2

Miscibility of CNF/CNW Nanocomposites Films

The compatibility of two polysaccharide compounds directly affects the physical and mechanical properties of the CNF/ CNW nanocomposites films. To determine their miscibility, the FTIR spectra of the CNF-2, CNW, and MIX-2 films were analyzed for band shifts, peak broadening, and relative intensity changes (in Fig. 4b and c). The characteristic peaks of MIX-2 at 3500 cm^{-1}, 2900 cm^{-1}, and 1650 cm^{-1} are ascribed to O–H, C–H, and C=O stretching, respectively. Unlike the other films, obvious changes can be found in the O–H characteristic peak of MIX-2. This could be due to there being more numerous hydrogen bonds formed in nanocomposite films by doping CNW.

In addition, the second derivation spectra were executed in the O-H region of MIX-2 film as shown in Fig. 4d. The absorbance bands in the range of 3600 cm^{-1} to 3000 cm^{-1} can be split into five regions. According to Minke and Blackwell (1978), cellulose and chitin contain intramolecular and intermolecular hydrogen bonds. In cellulose, an OH group at the C2 position forms an H-bond with an O6 atom of the adjacent molecular ring (O2-H···O6 intramolecular hydrogen bond), and another OH group at the C3 position forms an H-bond with an O5 atom of the adjacent molecular ring (O3-H···O5 intramolecular hydrogen bond). The OH at the C6 position forms an H-bond with an O3 atom of the neighbor chain (O6-H···O3' intermolecular hydrogen bond). Similarly, intermolecular hydrogen bonding in chitin can be marked as O(6)H···O(6'). In cellulose, the bonds vibration at 3548 and 3464 cm^{-1} were assigned to intermolecular O(2)H···O(6) and

O(3)H···O(5) H-bonds. The peak at 3383 cm^{-1} was due to the stretching of the intermolecular O(6)H···O(3') H-bonds (Moriana *et al*. 2014). In chitin, the peak at 3130 cm^{-1} was generally assigned to the intermolecular O(6)H···O(6') H-bonds. And the peak at 3262 cm^{-1} was assigned to the intermolecular C(2)NH···O(6') H-bonds, which is formed by NH group at the C2 position in chitins chain with the an O6 atom of the neighbor D-glucose ring (Wu *et al*. 2008). Hydrogen bonding interactions were evident in the mixed film.

Mechanical and Thermal Properties of Composite Films

The tensile strength, Young modulus, and the elongation break of the CNF, CNW, and MIX films were tested. The results were presented in Fig. 5a, b, and c. It was revealed that CNW film had the lower tensile strength and Young modulus in comparison to pure CNF films and composite films. On the contrary, the mechanical properties of these films mainly depended on polysaccharides sources (Chi *et al.* 2017). The crystal modulus of CNF was reported as 136 GPa to 150 GPa (Iwamoto *et al*. 2009), and the crystal modulus of α-chitin was only 41 GPa (Nishino *et al*. 1999). Therefore, the CNF films had a higher tensile strength and Young modulus than CNW film. Moreover, CNF-5 had the highest tensile strength and Young modulus. This was due to its high carboxyl content and relatively large aspect ratios in comparison with CNF-1 and CNF-2. The mechanical strength of the nanofilms decreased significantly when exposed into higher humidity condition (Table 2). However, the wet strength of the film increased after loading CNW, which was possibly due to the partially deacetylated CNW exposed to more amino groups and improvement of the formation of hydrogen bond structure between CNFs and CNWs in films.

Introducing CNW to the nanofilm led to a slight increase in tensile strength and Young modulus. The changes in tensile strength and Young modulus in MIX-1 and MIX-2 were due to the interfacial interaction, such as electrostatic interaction between cationic CNW and anionic CNF, hydrogen bonds between amino and hydroxyl groups. However, increasing the constituent of CNW to 50% or higher, the tensile strength and Young modulus decreased. This was because more CNW in the composite reduced its chemical binding with CNF.

Figure 5c shows the elongation of film samples. A slight increase of elongation could be observed in CNF films. However, the values of elongation decreased obviously by loading CNW in composite films. It was speculated that the rigidity of the charged polysaccharides might be responsible for this difference. Because the used α-chitin was inflexible and relatively rigid (Araki and Yamanaka 2014). Therefore, the network of the hybrid films was easily broken, especially in MIX-3.

The thermal degradation and pyrolysis behaviors of nanofilms were investigated by TGA. The weight loss curves of CNF-2, MIX-2, and CNW are shown in Fig. 5d. The first mass-loss regions of the film were from 25 °C to 200 °C. This was attributed to the release of water with a weight loss ratio of approximately 8.0 wt.% in the films. The second mass-loss region was between 200 °C to 400 °C. In this region, the weight was mainly lost due to the depolymerization of polysaccharide compounds. The formation of nano-scale cellulose resulted in a decrease in thermolysis temperature because the generated C6-carboxylate groups had a relatively lower thermal stability (Lavoine *et al.* 2016). Meanwhile, it was easier to decompose due to its lower polymerization degree of CNF. In addition, the corresponding temperatures at 50% mess loss of CNF-2, MIX-2 and CNW were 354.09 ºC, 368.27 ºC, and 375.12 ºC, respectively. Therefore, the thermal stability of MIX-2 was slightly improved by the addition of CNW.

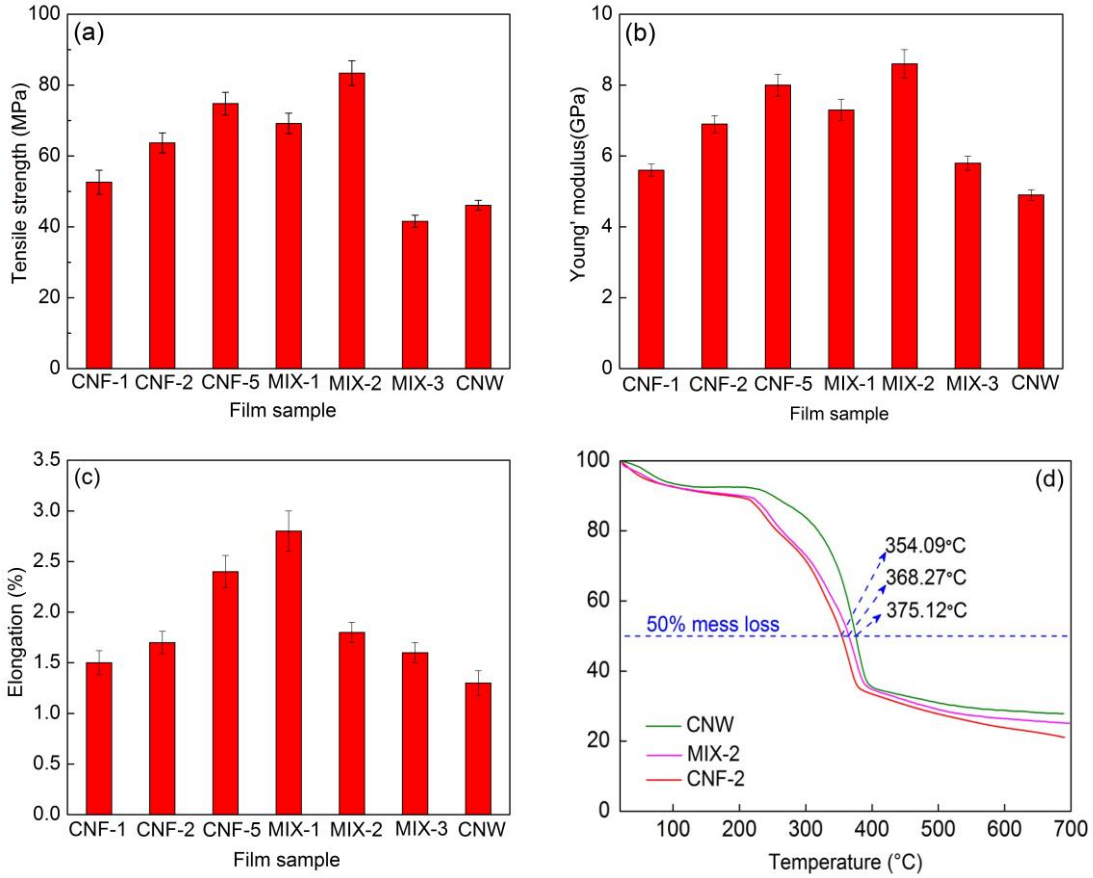

Fig. 5. Effect of CNW on the mechanical properties of mixed films (a) tensile strength, (b) Young modulus, (c) elongation at break, and (d) thermogravimetric curves of CNF-2, MIX-2, and CNW films

CONCLUSIONS

1. Wheat straw and chitin were prepared into nanofibers by TEMPO-oxidation and acid hydrolysis process, respectively. Zeta potential results indicated significant differences in suspending mechanism of CNF and CNW dispersions. The results also confirmed that a higher oxidation degree promoted the formation of a smaller size of fibers and better stability of CNF dispersions.
2. Based on the opposite surface charge characteristics between CNF and CNW, hybrid films were prepared, and their physical and mechanical properties could be improved due to interfacial interaction (*e.g.* electrical interaction and hydrogen bond). The tensile strength and Young modulus of the films increased with the loading of CNW. However, increasing the CNW content up to 50% negatively affected the physical properties of the hybrid films.
3. A homogenous nanoscale of CNF resulted in high transparency of films. The reduced transparency of the CNF/ CNW mixed film was attributed to larger scale of CNF/ CNW formed by physical interactions. The second derivation spectra in the O-H region in the FTIR indicated that the hydrogen bond was the main combination force between CNF and CNW in the hybrid films.

ACKNOWLEDGMENTS

The authors are grateful for the support of the China Postdoctoral Science Foundation (No. 2017T100633 and 2016M602472), the National Natural Science Foundation of China (No. 31600471), the Natural Science Foundation of Guangdong Province (No. 2015A030310369 and 2015A030313221), the Fundamental Research Funds for the Central Universities (2017MS087 and 2017ZD089), the 111 Plan and Guangdong Provincial Science and Technology Plan Projects (No. 2015B020241001), and the financial support of Science and Technology Plan Projects of Guangzhou city (Number: 201504010013, Name: Study on Quality Intelligent Control of Modern Paper Machine and Energy-saving Technology with Equipment).

REFERENCES CITED

Abdul, K. H. P. S., Saurabh, C. K., Adnan, A. S., Fazita, M. R. N., Syakir, M. I., Davoudpour, Y., Rafatullah, M., Abdullah, C. K., Haafiz, M. K. M., and Dungani, R. (2016). "A review on chitosan-cellulose blends and nanocellulose reinforced chitosan biocomposites - Properties and their applications," *Carbohydrate Polymers* 150, 216-226. DOI: 10.1016/j.carbpol.2016.05.028

And, M. P., and Dufresne, A. (2001). "Chitin whisker reinforced thermoplastic nanocomposites," *Macromolecules* 34(19), 6527-6530. DOI: 10.1021/ma002049v

Ansari, F., Johansson, M., Plummer, C. J. G., Berglund, L. A., and Galland, S. (2014). "Cellulose nanofiber network for moisture stable, strong, and ductile biocomposites and increased epoxy curing rate," *Composites Part A Applied Science and Manufacturing* 63(63), 35-44. DOI: 10.1016/j.compositesa.2014.03.017

Araki, J., and Yamanaka, Y. (2014). "Anionic and cationic nanocomposite hydrogels reinforced with cellulose and chitin nanowhiskers: Effect of electrolyte concentration on mechanical properties and swelling behaviors," *Polymers for Advanced Technologies* 25(10), 1108-1115. DOI:10.1002/pat.3361

Chandra, R., Takeuchi, H., and Hasegawa, T. (2012). "Methane production from lignocellulosic agricultural crop wastes - A review in context to second generation of biofuel production," *Renewable and Sustainable Energy Reviews* 16(3), 1462-1476. DOI: 10.1016/j.rser.2011.11.035

Chen, W., Yu, H., Li, Q., Liu, Y., and Li, J. (2011). "Ultralight and highly flexible aerogels with long cellulose I nanofibers," *Soft Matter* 7(21), 10360-10368. DOI: 10.1039/C1SM06179H

Chi, K., and Catchmark, J. M. (2017). "The influences of added polysaccharides on the properties of bacterial crystalline nanocellulose," *Nanoscale* 9(39), 15144-15158. DOI:10.1039/C7NR05615J

Da, S. P. D., Montanari, S., and Vignon, M. R. (2003). "TEMPO-mediated oxidation of cellulose III," *Biomacromolecules* 4(5), 1417-1425. DOI: 10.1021/bm034144s

Diop, C. I. K., Tajvidi, M., Bilodeau, M. A., Bousfield, D. W., and Hunt, J. F. (2017). "Isolation of lignocellulose nanofibrils (LCNF) and application as adhesive replacement in wood composites: Example of fiberboard," *Cellulose* 24(7), 3037-3050. DOI:10.1007/s10570-017-1320-z

Fang, Z., Zhu, H., Yuan, Y., Ha, D., Zhu, S., Preston, C., Chen, Q., Li, Y., Han, X., and Lee, S. (2014). "Novel nanostructured paper with ultrahigh transparency and

ultrahigh haze for solar cells," *Nano Letters* 14(2), 765-773. DOI: 10.1021/nl404101p

Huang, J., Zhu, H., Chen, Y., Preston, C., Rohrbach, K., Cumings, J., and Hu, L. (2013). "Highly transparent and flexible nanopaper transistors," *ACS Nano* 7(3), 2106-2113. DOI: 10.1021/nn304407r

Iwamoto, S., Kai, W., Isogai, A., and Iwata, T. (2009). "Elastic modulus of single cellulose microfibrils from tunicate measured by atomic force microscopy," *Biomacromolecules* 10(9), 2571-2576. DOI: 10.1021/bm900520n

Kaya, M., Asanozusaglam, M., and Erdogan, S. (2016). "Comparison of antimicrobial activities of newly obtained low molecular weight scorpion chitosan and medium molecular weight commercial chitosan," *Journal of Bioscience and Bioengineering* 121(6), 678-684. DOI: 10.1016/j.jbiosc.2015.11.005

Khalil, H. P. S. A., Bhat, A. H., and Yusra, A. F. I. (2012). "Green composites from sustainable cellulose nanofibrils - A review," *Carbohydrate Polymers* 87(2), 963-979. DOI: 10.1016/j.carbpol.2011.08.078

Kingkaew, J., Kirdponpattara, S., Sanchavanakit, N., Pavasant, P., and Phisalaphong, M. (2014). "Effect of molecular weight of chitosan on antimicrobial properties and tissue compatibility of chitosan-impregnated bacterial cellulose films," *Biotechnology and Bioprocess Engineering* 19(3), 534-544. DOI: 10.1007/s12257-014-0081-x

Kumar, A. M., Suresh, B., Das, S., Obot, I. B., Adesina, A. Y., and Ramakrishna, S. (2017). "Promising bio-composites of polypyrrole and chitosan: Surface protective and in vitro, biocompatibility performance on 316l ss implants," *Carbohydr. Polym.* 173, 121-130. DOI: 10.1016/j.carbpol.2017.05.083

Lavoine, N., Bras, J., Saito, T., and Isogai, A. (2016). "Improvement of the thermal stability of tempo-oxidized cellulose nanofibrils by heat-induced conversion of ionic bonds to amide bonds," *Macromol Rapid Commun* 37(13), 1033-1039. DOI:10.1002/marc.201600186

Li, M. C., Wu, Q. L., Song, K. L., Cheng, H. N., Suzuki, S., and Lei, T. Z. (2016). "Chitin nanofibers as reinforcing and antimicrobial agents in carboxymethyl cellulose films-Influence of partial deacetylation," *ACS Sustainable Chemistry and Engineering* 4(8), 4385-4395. DOI: 10.1021/acssuschemeng.6b00981

Li, Y., Zhu, H., Shen, F., Wan, J., Han, X., Dai, J., and Hu, L. (2014). "Highly conductive microfiber of graphene oxide templated carbonization of nanofibrillated cellulose," *Advanced Functional Materials* 24(46), 7366-7372. DOI: 10.1002/adfm.201402129

Li, Z., Yang, R., Yang, F., Zhang, M., and Wang, B. (2015). "Structure and properties of chitin whisker reinforced papers for food packaging application," *BioResources* 10(2), 2995-3004. DOI: 10.15376/biores.10.2.2995-3004

Liimatainen, H., Visanko, M., Sirviö, J. A., Hormi, O. E. O., and Niinimaki, J. (2012). "Enhancement of the nanofibrillation of wood cellulose through sequential periodate–chlorite oxidation" *Biomacromolecules* 13(5), 1592-1597. DOI: 10.1021/bm300319m

Malho, J. M., Ouelletplamondon, C., Ikkala, O., Burgert, I., and Linder, M. B. (2014). "Enhanced plastic deformations of nanofibrillated cellulose film by adsorbed moisture and protein-mediated interactions," *Biomacromolecules* 16(1), 311-318. DOI: 10.1021/bm501514w

Marko, P., Martin, M., Ulla, V., Mattipaavo, S., Pekka, S., and Ritva, S. (2008). "X-ray microdiffraction reveals the orientation of cellulose microfibrils and the size of cellulose crystallites in single Norway spruce tracheids," *Trees* 22(1), 49-61. DOI: 10.1007/s00468-007-0168-5

Minke, R., and Blackwell, J. (1978). "The structure of α-chitin," *Biochimica Et*

Biophysica Acta 120(2), 167-181. DOI: 10.1016/0022-2836(78)90063-3

Moriana, R., Vilaplana, F., Karlsson, S., and Ribes, A. (2014). "Correlation of chemical, structural, and thermal properties of natural fibres for their sustainable exploitation," *Carbohydrate Polymers* 112(2), 422-431. DOI: 10.1016/j.carbpol.2014.06.009

Mututuvari, T. M., and Tran, C. D. (2014). "Synergistic adsorption of heavy metal ions and organic pollutants by supramolecular polysaccharide composite materials from cellulose, chitosan, and crown ether," *Journal of Hazardous Materials* 264, 449-459. DOI: 10.1016/j.jhazmat.2013.11.007

Nair, S. S., Kuo, P. Y., Chen, H., and Yan, N. (2017). "Investigating the effect of lignin on the mechanical, thermal, and barrier properties of cellulose nanofibril reinforced epoxy composite," *Industrial Crops & Products* 100, 208-217. DOI:10.1016/j.indcrop.2017.02.032

Naseri, N., Mathew, A. P., Girandon, L., Fröhlich, M., and Oksman, K. (2014). "Porous electrospun nanocomposite mats based on chitosan-cellulose nanocrystals for wound dressing- Effect of surface characteristics of nanocrystals," *Cellulose* 22(1), 521-534. DOI: 10.1007/s10570-014-0493-y

Nishino, T., Matsui, R., and Nakamae, K. (1999). "Elastic modulus of the crystalline regions of chitin and chitosan," *Journal of Polymer Science Part B Polymer Physics* 37(11), 1191-1196. DOI: 10.1002/(SICI)1099-0488(19990601)37:11<1191::AID-POLB13>3.0.CO;2-H

Qiu, C., Hu, X., Li, L., Yang, X., Zhao, M., and Ren, J. (2016). "Effect of transglutaminase cross-linking on the conformational and emulsifying properties of peanut arachin and conarachin fractions," *European Food Research and Technology* 2016,1-8. DOI: 10.1007/s00217-016-2804-z

Saito, T., Hirota, M., Tamura, N., Kimura, S., Fukuzumi, H., Heux, L., and Isogai, A. (2009). "Individualization of nano-sized plant cellulose fibrils by direct surface carboxylation using TEMPO catalyst under neutral conditions," *Biomacromolecules* 10(7), 1992-1996. DOI: 10.1021/bm900414t

Singh, N., Rahatekar, S. S., Koziol, K. K., Ng, T. S., Patil, A. J., Mann, S., Hollander, A. P., and Kafienah, W. (2013). "Directing chondrogenesis of stem cells with specific blends of cellulose and silk," *Biomacromolecules* 14(5), 1287-1298. DOI: 10.1021/bm301762p

Shen, X., Shamshina, J. L., Berton, P., Gurau, G., and Rogers, R. D. (2016). "Cheminform abstract: Hydrogels based on cellulose and chitin: Fabrication, properties, and applications," *Cheminform* 47(9), 53-75. DOI: 10.1039/C5GC02396C

Toivonen, M. S., Kurki-Suonio, S., Schacher, F. H., Hietala, S., Rojas, O. J., and Ikkala, O. (2015). "Water-resistant, transparent hybrid nanopaper by physical cross-linking with chitosan," *Biomacromolecules* 16(3), 1062-1071. DOI: 10.1021/acs.biomac.5b00145

Wang, B., Chen, K., Yang, R., Yang, F., and Liu, J. (2014). "Stimulus-responsive polymeric micelles for the light-triggered release of drugs," *Carbohydrate Polymers* 103C(1), 510-519. DOI: 10.1016/j.carbpol.2013.12.062

Wang, W., Bo, S., Li, S., and Qin, W. (1991). "Determination of the Mark-Houwink equation for chitosans with different degrees of deacetylation," *International Journal of Biological Macromolecules* 13(5), 281-285. DOI: 10.1016/0141-8130(91)90027-R

Wu, Y., Sasaki, T., Irie, S., and Sakurai, K. (2008). "A novel biomass-ionic liquid platform for the utilization of native chitin," *Polymer* 49(9), 2321-2327. DOI: 10.1016/j.polymer.2008.03.027

Yano, H., Sugiyama, J., Nakagaito, A. N., Nogi, M., Matsuura, T., Hikita, M., and Handa, K. (2005). "Optically transparent composites reinforced with networks of bacterial nanofibers," *Advanced Materials* 1(2), 153-155. DOI:10.1002/adma.200400597

Zerson, M., Neumann, M., Steyrleuthner, R., Neher, D., and Magerle, R. (2016). "Surface structure of semicrystalline naphthalene diimide–bithiophene copolymer films studied with atomic force microscopy," *Macromolecules* 49(17), 6549-6557. DOI:10.1021/acs.macromol.6b00988

Zhang, H., Gao, X., Chen, K. L., and Liu, Q. X. (2016). "Maximizing the yield of water-soluble cellouronic acid sodium salt with high carboxyl content by 4-acetamide-TEMPO mediated oxidation of parenchyma cellulose from bagasse pith," *Iranian Polymer Journal* 25(5), 465-474. DOI: 10.1007/s13726-016-0438-4

Zhang, K., Fischer, S., Geissler, A., and Brendler, E. (2012). "Analysis of carboxylate groups in oxidized never-dried cellulose II catalyzed by TEMPO and 4-acetamide-TEMPO," *Carbohydrate Polymers* 87(1), 894-900. DOI: 10.1016/j.carbpol.2011.08.090

Zhang, Y., Chen, K., Wan, J., Zhuo, H., Li, J., Yang, R., Yang, W., Wang, F., and Wang, B. (2016). "Thermal dynamics and a comparison of the thermal stability of various non-wood pulps," *BioResources* 11(1), 2138-2151. DOI: 10.15376/biores.11.1.2138-2151

Zheng, G., Cui, Y., Karabulut, E., Wågberg, L., and Hu, H. Z. L. (2013). "Nanostructured paper for flexible energy and electronic devices," *Mrs Bulletin* 38(4), 320-325. DOI: 10.1557/mrs.2013.59

Article submitted: September 27, 2017; Peer review completed: December 29, 2018; Revised version received: February 27, 2018; Accepted: February 28, 2018; Published: March 6, 2018.
DOI: 10.15376/biores.13.2.3030-3044